# Salt Concentration Effects in Planar Light-Emitting Electrochemical Cells

**ARTICLE** *in* ADVANCED FUNCTIONAL MATERIALS · MAY 2011

Impact Factor: 11.81 · DOI: 10.1002/adfm.201002360

# Salt Concentration Effects in Planar Light-Emitting Electrochemical Cells

*Stephan van Reenen, Piotr Matyba, Andrzej Dzwilewski, René A. J. Janssen, Ludvig Edman, and Martijn Kemerink**

**Incorporation of ions in the active layer of organic semiconductor devices may lead to attractive device properties like enhanced injection and improved carrier transport. In this paper, we investigate the effect of the salt concentration on the operation of light-emitting electrochemical cells, using experiments and numerical calculations. The current density and light emission are shown to increase linearly with increasing ion concentration over a wide range of concentrations. The increasing current is accompanied by an ion redistribution, leading to a narrowing of the recombination zone. Hence, in absence of detrimental side reactions and doping-related luminescence quenching, the ion concentration should be as high as possible.**

## 1. Introduction

Charge carrier transport in organic semiconductors is often limited by poor injection and/or a low conductivity. The latter typically results from a low carrier mobility and a low charge density that is limited by the build-up of space charge. The effects of space charge are relatively severe due to the low dielectric constant in organic semiconductors, resulting in relatively weak screening of charge carriers. In light-emitting electrochemical cells (LECs),[1–3] these transport limitations are strongly reduced by the incorporation of mobile ions into the semiconductor. This is attained by mixing the semiconductor with a solid electrolyte, so that ions can move freely through the active layer during operation.[4] Upon application of a bias voltage ($V_{bias}$) larger than the bandgap of the organic semiconductor ($E_g$), polymer chains are reduced or oxidized by the injection of electrons and holes into the semiconductor. The cations and anions stabalize this redox reaction by serving as counterions for the reduced and oxidized chains. This electrochemical doping process prevents the formation of space charge when electrons or holes are injected from the contacts into the semiconductor. The resultant enhanced carrier density (and mobility when the mobility is density dependent)[5] is concomitant with increased conductivity and enables enhanced device currents and light output.[6,7] The large conductivity also opens up the opportunity to fabricate wide interelectrode-gap LECs in a planar configuration.[8,9] Such cells allow probing by surface techniques like scanning Kelvin probe microscopy (SKPM).[10–13]

As well as improving carrier transport, the ions also improve the injection of charge carriers past relatively large injection barriers for $V_{bias} > E_g$. This is done by the formation of electric double layers (EDLs). Oppositely charged ions are attracted by the positive and negative electrodes and accumulate at the electrode interfaces forming charged sheets. The large electric fields in the EDLs strongly reduce the barrier widths for carrier injection.[14–18]

Despite these obvious advantages over conventional LEDs, the interest in LECs has mainly been academic. This can be accounted for by a relatively short lifetime[6] and long response time.[19] The former can be attributed to electrolyte-induced side reactions at the electrode interfaces[20] and the emission zone,[21] whereas the latter is a result of the slowness of the doping process because of the relatively low ionic mobility. Salvation of this problem has been achieved by fixing the ions in a favorable (re)distribution by either irreversible chemical reactions[22–27] or temperature control.[28–31] Another detrimental effect of large ion concentrations can be doping-induced exciton quenching.[32] In optimized LECs, the recombination of excitons takes place in a narrow region sandwiched in between p- and n-type doped regions: the p–n junction.[11] Hence, exciton quenching is highly probable and will negatively affect the quantum efficiency of LECs.[32]

All mentioned advantages and disadvantages of LECs are directly related to the presence of ions in the active layer. Therefore, it is of utmost importance to understand the influence of the ion concentration on the LEC characteristics. Ideally an LEC contains sufficient ions to facilitate efficient carrier injection and conduction, but insufficient to suffer from detrimental effects like short operational life times and decreased efficiency. A few studies have already aimed at understanding the influence of the ion concentration in LECs. Fang et al.[33] have shown that in planar LECs with a relatively low ion concentration the doping fronts come to a halt before making contact, so no sharp p–n junction is formed. Other work on sandwich cell LECs with relatively low ionic content has shown improved lifetimes in combination with efficient injection.[32,34–36]

S. van Reenen, Dr. A. Dzwilewski, Prof. R. A. J. Janssen, Dr. M. Kemerink
Department of Applied Physics
Eindhoven University of Technology
PO Box 513, 5600 MB, Eindhoven, The Netherlands
E-mail: m.kemerink@tue.nl
P. Matyba, Prof. L. Edman
Department of Physics
Umeå University
SE-901 87 Umeå, Sweden

**DOI: 10.1002/adfm.201002360**

Here, we report the results of transient experiments carried out on planar LECs of which the active layer is a mixture of the light emitting polymer "superyellow" (SY-PPV) and an electrolyte consisting of poly(ethylene oxide) (PEO) and the salt potassium triflate ($KCF_3SO_3$). The salt concentration was varied to study its effect on the device operation of the LEC. SKPM was performed to study the evolution of the electrostatic potential, complemented by UV-excited photoluminescence (PL) measurements to monitor the electrochemical doping progression. In addition, numerical calculations were used to interpret the effects of a reduced ion concentration on the measured current, potential, and doping transients. The results show that in an ideal LEC, i.e., in the absence of electroluminescence quenching and side reactions, the current density and light output at fixed bias are linearly proportional to the ion concentration over many orders of magnitude.

## 2. Results and Discussion

### 2.1. Experimental Characterization

Two sets of planar LECs with different SY-PPV/PEO/$KCF_3SO_3$ weight ratios were prepared: ion-rich devices (1:1.35:0.25) and ion-poor devices (1:1.35:0.06). To study the difference in doping during device operation, PL measurements were carried under UV illumination of the active layer. As both p- and n-type doping quench the UV-excited PL, the doped regions appear darker than undoped regions. The photographs are shown in **Figure 1**a and b. In Figure 1c–e schematic drawings of the anion and cation concentration distributions in LECs are shown before operation (c), during doping front progression (d), and in steady state (e). In unbiased, pristine devices the anions and cations are homogeneously distributed across the active layer (see Figure 1c). After application of a bias voltage, charges are injected. The injection initiates doping of the active layer, starting from the electrodes. The p- ($a^-p^+$) and n-type ($c^+p^-$) doping fronts propagate towards each other while splitting the available paired ions ($a^-c^+$) for the doping process (see Figure 1d). Ultimately, all of the anions and cations are used for doping of the polymer and are separated from each other (see Figure 1e).[11] In Figures 1a and b, this doping process was investigated in ion-rich and ion-poor LECs. At $t = 0$, a bias voltage of 8 V was applied to the pristine devices. In the ion-rich device (Figure 1a) p- and n-type doping initiate from the anode and cathode respectively. These doping fronts then propagate towards each other and meet at $t = 9$ s. After that, light emission is observed, originating from electroluminescence (last picture of Figure 1a). In the ion-poor device, doping fronts also form (Figure 1b). However, the doping fronts never meet as the n-type doping front only moves a short distance away from the negative contact and the p-type doping front stops at the centre of the active layer ($t = 600$ s). Eventually, the p-type doping front seems to retract somewhat towards the anode and the boundary between the p-doped and undoped region becomes less sharp. No electroluminescence was observed in the ion-poor LEC.

To obtain better insight into these characteristic results, SKPM was performed on similar devices. SKPM monitors the electrostatic potential in the active layer during operation of the LEC. Potential profiles of ion-rich and ion-poor devices operating at steady state are shown in **Figure 2**a and b. The device was alleged to be at steady state when the potential profile did not significantly evolve anymore. The UV-excited PL measurements during steady state operation on similar devices have been added to the background of the graphs to enable

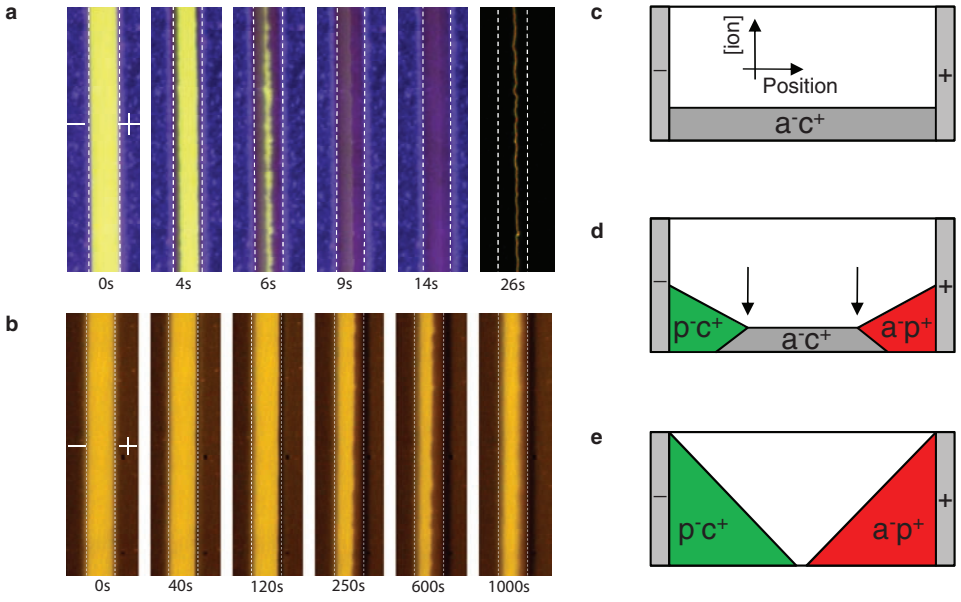


**Figure 1.** Photographs of planar Au/{SY-PPV + PEO + $KCF_3SO_3$}/Au LECs with an interelectrode gap of ~90 µm during operation at $V_{bias} = 8$ V and $T = 333$ K. Two different SY-PPV:PEO:$KCF_3SO_3$ weight ratios were used: a) 1:1.35:0.25 – ion-rich and b) 1:1.35:0.06 – ion-poor. c–e) The ionic redistribution and doping process is schematically shown in. $a^-$ (red area), $c^+$ (green area), $p^-$, and $p^+$ refer to anions, cations, reduced polymer, and oxidized polymer respectively. In the gray regions, the anion and cation concentrations are equal. The arrows in (d) indicate the position of the doping fronts.

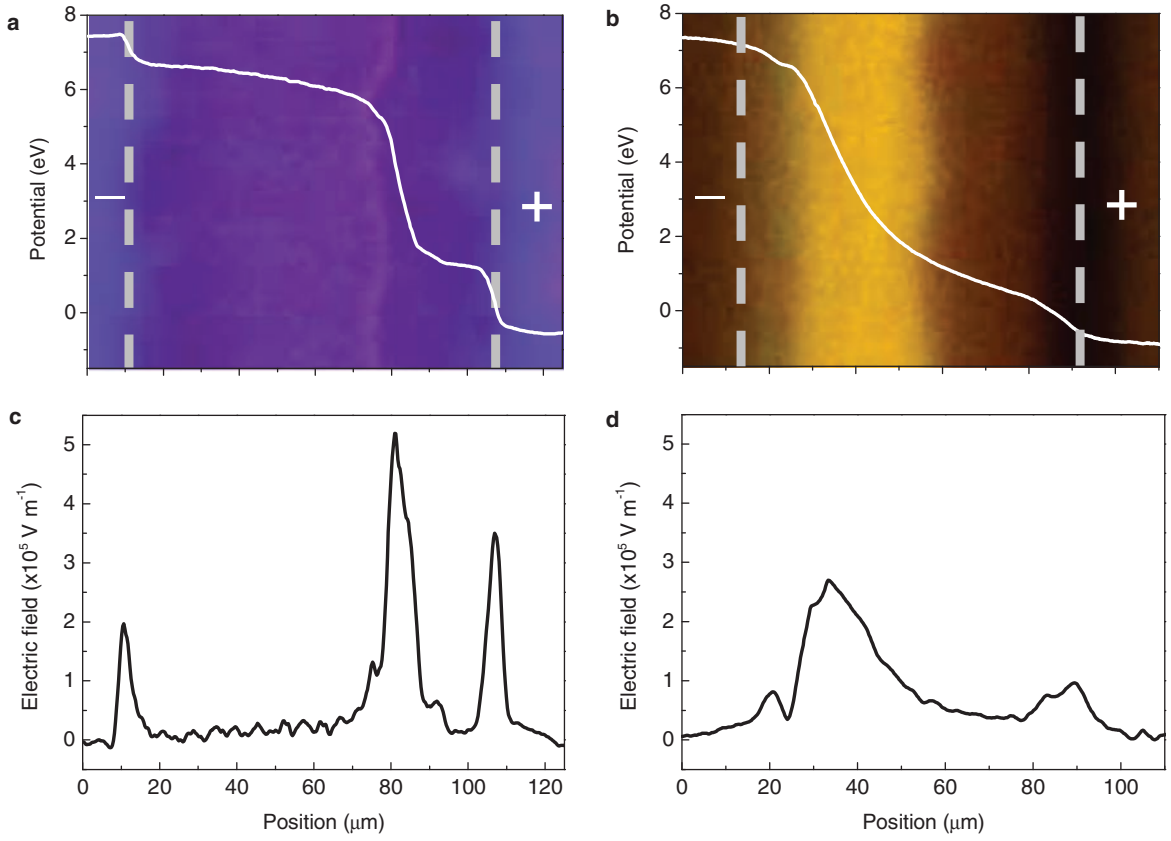


**Figure 2.** a,b) Electrostatic potential and c,d) field profiles in planar LECs during operation at $V_{bias}$ = 8 V with weight ratios SY-PPV:PEO:$KCF_3SO_3$ 1:1.35:0.25 (a and c) and 1:1.35:0.06 (b and d). The photographs behind the graphs (a and b) are UV-excited PL images recorded at steady state, on the same horizontal scale. The electrode interfaces are indicated by the gray dashed lines.

comparison. The corresponding electrostatic field profiles are shown in Figures 2c and d for the ion-rich and ion-poor device, respectively.

Doping strongly decreases the resistivity of the semiconductor. Consequently, a smaller electric field is necessary in stronger doped regions to conduct the same amount of current. The intrinsic junction separating the p- and n-doped regions has a basically constant, higher resistivity and hence, requires a larger electric field to maintain a constant current at steady state. The resulting peak in the electric field profile is clearly observed in Figure 2c and d, with the p–n junction located around $x$ = 85 and $x$ = 40 μm, respectively. These positions clearly correlate with the UV-excited PL measurements in the background of Figure 2a and b, with the p–n junction coinciding with the emission zone for the ion-rich device and with the bright, unquenched region for the ion-poor device. Furthermore, in Figure 2a and c, regions of relatively large electric field are observed at the electrode interfaces ($x$ = 10 and 110 μm): the electric double layers. Similar high-field regions were identified in the ion-poor LEC (see Figure 2b and d) at $x$ = 20 and $x$ = 90 μm.

Comparison of Figure 2a,c and b,d reveals the following changes in the LEC due to a decreased ion concentration: i) the junction region width has increased, concomitant with a decreased electric field in the junction; ii) the electric field in the doped regions has increased and iii) the potential drop at the electrode interfaces has decreased. A detailed discussion of these observations is given later in this manuscript.

In addition to the steady state potential profiles, transient potential profiles were measured, as shown in **Figure 3**a and b for the ion-rich and ion-poor device, respectively. The arrows indicate the temporal trend of the potential profile evolution. In the ion-rich device, the EDLs form faster than the time resolution of the SKPM experiment of 10 s. Moreover, during the first potential measurement at $t$ = 10 s light emission was already observed in a similar device (see Figure 1a). Therefore, we may assume that the potential profile evolution shown here mainly reflects the saturation of doping after collision of the doping fronts, which is consistent with the observation that the light emission intensity from the p–n junction increases with time *after* the initial junction formation, as shown in Figure 1a and in a previous study.[37] This saturation is further indicated by the decreasing electric field ($-dV/dx$) in the doped regions and the increasing field in the junction region. Importantly, a comparison of Figure 1a and Figure 3a indicates that light emission already takes place from a narrow region even before the sharp potential drop has arisen. Moreover, if recombination does take place in the adjacent doped regions, the resultant light emission could be quenched by doping and therefore, would not be observed.

Where the LEC contains relatively few ions (Figure 3b), small EDLs are formed and mainly p-type doping is observed.

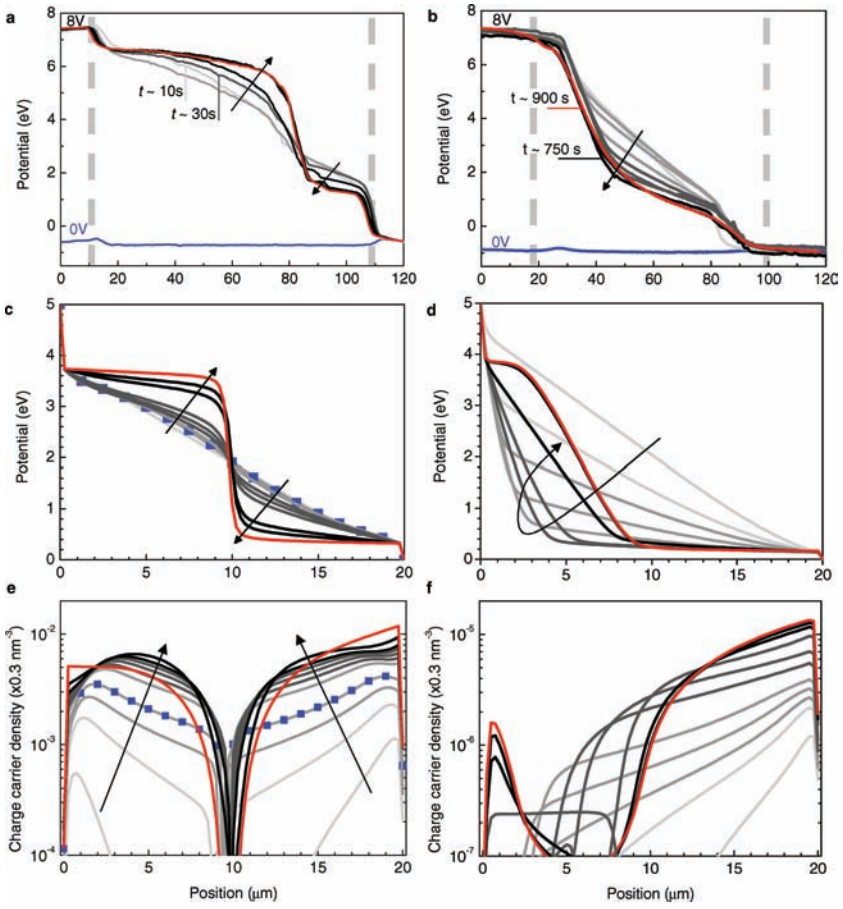


**Figure 3.** Transient potential profiles from experiments and calculations as well as calculated charge carrier density profiles. The experimentally determined profiles are from LECs with a SY-PPV:PEO:$KCF_3SO_3$ weight ratio of a) 1:1.35:0.25 – ion-rich and b) 1:1.35:0.06 – ion-poor. The numerically determined profiles are from LECs with an ion concentration of c–e) $1.5 \times 10^{-3}$ ions nm$^{-3}$ and d–f) $1.5 \times 10^{-6}$ ions nm$^{-3}$. The red lines denote the steady state potential profile and the blue lines in (a) and (b) the profiles taken at $V_{bias} = 0$ V. The black arrows accentuate the change of the profiles in time. The lines marked by blue squares indicate that the n-type and p-type doping fronts have met. The electrode interfaces are indicated by gray dashed lines.

For this device, the potential profiles could be measured in similar time intervals as the PL measurements shown in Figure 1b. The junction region is broader and includes the region close to the negative contact, indicating the absence of significant n-type doping. Comparison of the last two potential traces shown in black and red indicates that the transition from the p-doped region to the junction region becomes less sharp in time. A similar transition was already observed in the final two pictures in Figure 1b.

### 2.2. Numerical Calculations

In order to complement these experimental findings, numerical calculations were carried out to gain insight into the physical processes underlying the observed trends. A 1D model (see Supplementary Information for details) was used to calculate the potential profile evolution for LECs with a high and low ion density of $1.5 \times 10^{-6}$ and $1.5 \times 10^{-3}$ ions nm$^{-3}$ respectively. Since the length scale of the phase separation between electrolyte, salt and conjugated polymer is much smaller than the length scales of interest in this work, phase separation is excluded from the model (see Supplementary Information for AFM images and further discussion), The modeling results are shown in Figure 3c and d. Corresponding carrier density profiles are shown in Figure 3e and f for the high and low ion density simulations respectively. In the bulk, the carrier density equals the difference between the anion and cation density because of charge neutrality in the doped regions (see also Figure S5 in the Supporting Information).

Firstly, we consider the ion-rich LEC. The modeled potential profiles show that after formation of EDLs, no significant change occurs in the potential profile during progression of doping through the active layer (light gray lines in Figure 3c and e). After both doping regions make contact (the corresponding profiles are indicated by blue squares), doping continues to saturate via the continued redistribution of ions. During doping of the active layer, ions are electrostatically compensated by electrons or holes.[11] Therefore, not all ions move towards the electrodes to completely screen the bulk from the externally applied field. A consequence of the saturation of the doping is the formation of a thin high-field region in the bulk: the p–n junction. The modeling shows that progression of doping is not necessarily visible in the potential evolution throughout the LEC. Furthermore, it indicates that the typical steady state potential profile (see Figure 2a) only appears when doping reaches its saturation point and not when the doping fronts meet, highlighted by the initiation of light-emission (compare Figure 3c and e). This is in agreement with the observed experimental behavior (see Figure 3a and Figure 1a). In the model, the formation of a sharp potential drop in the junction region is related to removal of ions from the junction region. The time needed for this removal is given by the speed of depletion of anions (cations) from the n (p) doped region (see Figure 1c–e).

Further comparison of experiment and model shows a difference in junction position. In the model, the junction is positioned in the centre of the active layer, in contrast with the experiment. The asymmetry of the injection barriers hardly affects the junction position in the model. The discrepancy with experiment is attributed to the absence of charge traps and side-reactions[20] and/or to the fact that the mobilities of holes and electrons were set equal in the model. Apart from the junction position, the simulation of an ion-rich LEC shows a qualitatively similar potential profile evolution as the real device.

The potential profile evolution in ion-poor LECs as determined by modeling (Figure 3d) and experiments (Figure 3b) also shows qualitatively similar behavior. In the model, the device has difficulty to form a good, i.e., a non-limiting or Ohmic contact at the negative electrode, as can be seen from the delayed formation of an n-type doped region ($x$ = 0–3 µm; see Figure 3f). This is due to the small amount of cations available to form an EDL at the negative contact, which has the largest injection barrier. Consequently, hole injection and subsequent p-type doping start far ahead of electron injection and n-type doping, as also experimentally observed (Figure 1b). In addition to this effect, the occurrence of side-reactions in real devices, which are known to predominantly occur at the negative electrode,[38] are a probable additional reason for the difficult injection of electrons that is observed in Figure 1b and Figure 3b. In both the model and the experiment, a moderately high-field junction region arises over a broad region relatively close to the negative contact.

To gain more insight into the effects of a reduced ion concentration in LECs, simulations were performed for ion densities ranging from $2 \times 10^{-6}$ nm$^{-3}$ to $1 \times 10^{-1}$ nm$^{-3}$. The steady state potential and electric field profiles are shown in **Figure 4**a and b, respectively. In Figure 4c, the absolute difference between anion and cation density is shown throughout the active layers. In the bulk, this difference is directly related to the doping density since charge neutrality demands that differences in ionic concentrations are compensated by electrons or holes. At the electrode interfaces the ion density also comprises unpaired ions, which do not contribute to doping, but rather are responsible for EDL formation.

For each value of $c_0$, the LEC operates according to the electrochemical doping model: at the interfaces ($x$ = 0 and 20 µm) EDLs are identified, closing in p- and n-type doping regions with a p–n junction in between.[11] Multiple trends can be discerned for decreasing $c_0$, which can be identified also in the experimental data in Figure 2 and 3. First of all, the p–n junction region width increases, whereas the potential drop at this junction shows only a minor increase. The result is that the electric field in this region decreases (see Figure 4b). Secondly, the width of the doped regions as well as the degree of doping decreases, while the electric field in these regions is enhanced. Lastly, the EDLs are affected, as the potential drop at the interfaces decreases for decreasing $c_0$. These phenomena are interconnected. Since the majority of ions is used for doping, the doping density and concomitantly, the conductivity in the doped regions decreases almost linearly upon lowering of $c_0$. Hence, the current density also declines linearly, as shown in **Figure 5**. Because of current continuity, this decline implies that the injection of charges must be decreased as well; otherwise, a surplus of injected carriers would form behind the EDLs. To this end, the strength of the EDLs is decreased, which results in larger effective injection barriers and lower charge injection. Finally, the fact that the width of the junction region

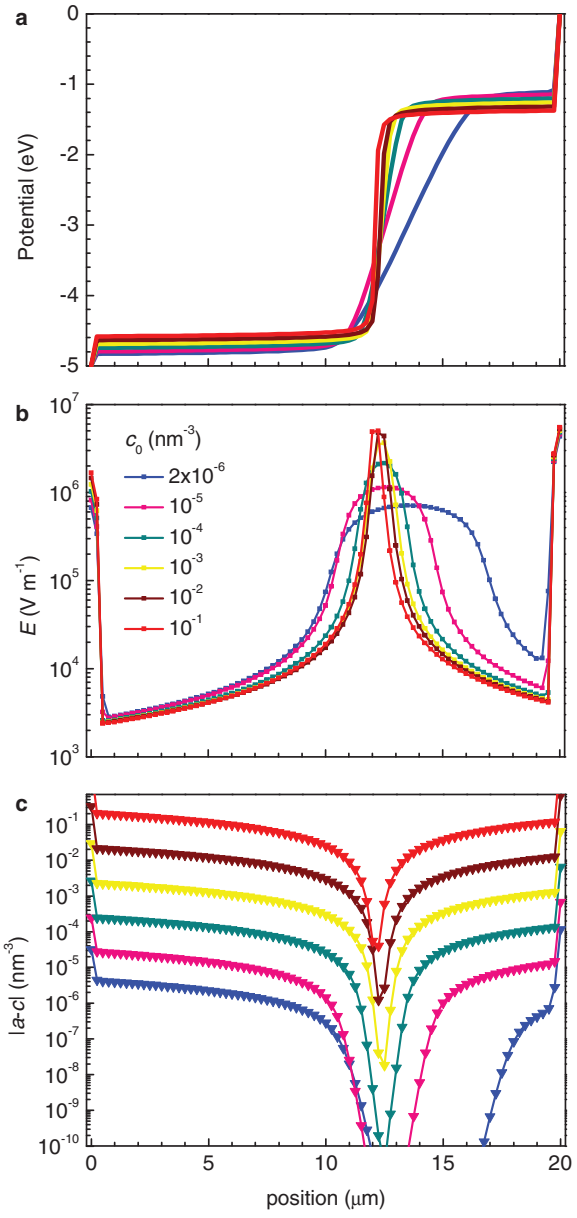


**Figure 4.** a) Electrostatic potential, b) field, and c) ionic density profiles in modeled LECs during operation in steady state for different initial ion concentrations ($c_0$, given in the legend).

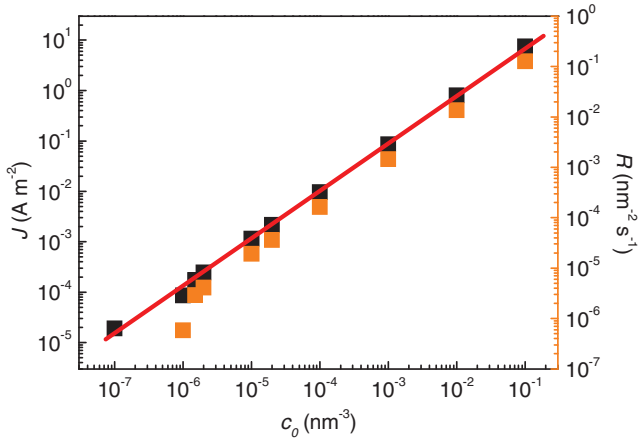


**Figure 5.** The steady state current density $J$ and recombination rate $R$ for different $c_0$. The red line follows the relation $J = A \times c_0$ for an arbitrary value of $A$, serving as a visual guide.

increases is also related to current continuity; the electric field, being proportional to the current through the junction, needs to be decreased by increasing the width of the junction region when the device current goes down. The mechanism outlined above shows that in LECs, the availability of ions to dope the conjugated polymer determines the potential profile both in the bulk and at the interfaces.

Another important result of the modeling presented here is the linear increase in the current density for increasing $c_0$, as shown in Figure 5. In principle, this implies that the presence of as much ions as possible is favorable for device performance. This is only true if all injected charge carriers recombine. In the modeling, the internal quantum efficiency is 100% as all carriers recombine in between the doped regions. In contrast to real devices, the model ignores doping-induced exciton quenching and spatial competition between the conjugated polymer, the electrolyte, and the ions. At some ion concentration, these two processes will start to adversely affect the radiative recombination efficiency, resulting in an upper limit for the allowable ion concentration.

In order to further determine the similarity between model and experiment, the measured and modeled current transients are presented in **Figure 6**. Characteristic features in both the high and low ion-density curves can be decomposed in an ionic and electronic contribution. Since the contacts are initially non-injecting, the current density at $t = 0$ can be attributed to the redistributing ions in the active layer. Thereafter, this contribution continuously declines due to ion pile-up at the electrodes and a decrease in the bulk field because of the resulting EDL formation. When EDLs are being formed, injection of electrons and holes is enhanced, resulting in an increasing electronic current. This rise is observed in all four current transients and the resulting maximum in current is marked by the arrows in Figure 6. Following this rise, a second decrease in the current density, now related to a decrease in the electronic current, is observed. After the onset of current injection from the contacts, a large fraction of the electronic current is 'consumed' for doping the device, i.e., used to compensate space charges resulting from the further separation of anions and cations. When this doping process is completed, the electronic current decreases. At steady state, anions and cations have been fully separated into p- and n-type doped regions, separated by a relatively sharp potential drop in the junction region; see Figure 1, 3 and 6. In the modeled LECs, the steady state current consists of an electronic contribution only; the ionic current has vanished due to the ion blocking electrodes and the absence of generation and recombination of ions. In principle, the same holds for the real LECs, although a minor ionic contribution from regions outside the inter-electrode gap, having a longer settling time due to the larger distances involved, cannot be excluded.

One of the major setbacks of LECs is the relatively long response time. The present experimental results, as well as those by Fang et al.,[33] show that a decrease in $c_0$ leads to an increase in the response time in LECs. The same is observed in modeled LECs (Figure 6) in which the ion concentration becomes so low that the formation of EDLs is affected and delayed. This is observed at the cathode in Figure 3d. However, current transients accompanying the simulations presented in Figure 4 reveal that when EDL formation is not hindered, the response time is independent of $c_0$; see also Supporting Information Figure S6. This difference between model and experiment suggests that processes omitted in the model cause the longer response time of low ion concentration LECs. In the model, the redistribution of ions is limited by the cations (anions) being transported from the p (n) doped region to the n (p) doped region. The latter is only controlled by the (field driven) drift current, and should therefore be independent of concentration, unless e.g., side reactions hinder the movement of ions. Alternatively, it is conceivable that the ionic mobility is concentration dependent. In either case, these results indicate that the use of a high ion density enhances the turn-on time.

So far, no comments have been made regarding the discrepancy between the ion concentration used in the model and the nominal salt concentration in the active layer during experiments. In the transient modeling presented in Figure 3c,d and 6a,b, the initial ion concentrations were chosen to be $1.5 \times 10^{-3}$ and $1.5 \times 10^{-6}$ nm$^{-3}$ for the high and low ion-density device, respectively. The nominal salt concentrations in the experiments were $3.0 \times 10^{-1}$ and $0.7 \times 10^{-1}$ nm$^{-3}$, respectively. The latter concentration difference of a factor of ~4 resulted in a decrease in the steady state current by a factor ~$10^3$: 1.5 µA for the ion-rich device and 0.4 nA for the ion-poor device. As shown in Figure 5, changing the initial ion concentration by a factor $10^3$ in the model leads to a change in the calculated current density by the same factor $10^3$. Also, the change in the modeled potential profile is similar to the change that is observed experimentally.The only way to achieve qualitatively similar current transients and potential profiles in the model and the experiment is by using three orders of magnitude difference between high and low ion concentrations in the model. These results imply that the effective initial *mobile* ion density in a real LEC is a highly nonlinear function of the salt concentration. We speculate that this behavior is related to the effective loss of ions in side-reactions[20,21] and/or to the existence of immobile ions locked up in crystalline PEO phases.[39,40]

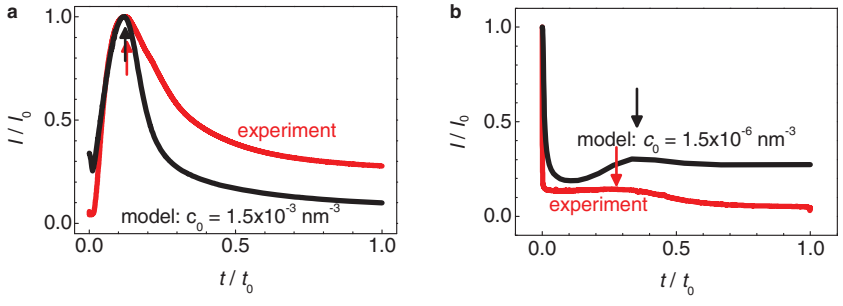


**Figure 6.** Current transients of planar Au/{SY-PPV + PEO + $KCF_3SO_3$}/Au LECs with an interelectrode gap of ~90 µm during operation at $V_{bias}$ = 8 V. Two different SY-PPV:PEO:$KCF_3SO_3$ weight ratios were used: a) 1:1.35:0.25 – ion-rich and b) 1:1.35:0.06 – ion-poor. The modeled current transients are from LECs with an initial homogeneous ion concentration ($c_0$) as specified in the figures. [$I_0$, $t_0$] in (a) is [5 µA, 150 s] for the experiment and [1.8 Am$^{-2}$, 54 s] for the model and in (b), [5 nA, 1200 s] for the experiment and [0.15 mAm$^{-2}$, 300 s] for the model.

## 3. Conclusions

By combination of experiments and numerical modeling, insight is gained regarding the function of ions in planar light-emitting electrochemical cells. An increase in the initial ion concentration results in an increased steady state current density and recombination rate in the LEC, due to the enhanced conductivity of the active layer by electrochemical doping. Concomitantly, injection is enhanced and the recombination zone is narrowed. Hence, from a device modeling point of view, optimal performance in terms of light output at a given bias requires the use of an as high as possible ion concentration. In real devices, adverse effects like doping-induced exciton quenching, side-reactions, and a finite solubility may put an upper limit to the optimal ion concentration.

## 4. Experimental Section

*Device Preparation*: For the conjugated polymer in the active layer, we used a phenyl-substituted poly(p-phenylene vinylene) copolymer (SY-PPV, Merck, catalogue number PDY-132), commonly termed "superyellow". Poly(ethylene oxide) (PEO, $M_w = 5 \times 10^5$ g mol$^{-1}$, Aldrich) was used as received. The salt potassium trifluoromethanesulfonate ($KCF_3SO_3$, 98%, Aldrich) was dried at 473 K under vacuum before use. SY-PPV was dissolved (5 mg mL$^{-1}$) in cyclohexanone (>99%, anhydrous, Aldrich). PEO and $KCF_3SO_3$ were dissolved separately (10 mg mL$^{-1}$) in cyclohexanone (>99%, anhydrous, Aldrich). These solutions were mixed together in a weight ratio of SY-PPV/PEO/$KCF_3SO_3$ = 1:1.35:0.25. For the fabrication of ion-poor devices, a weight ratio of 1:1.35:0.06 was used. These blend solutions were thereafter stirred on a magnetic hot plate at a temperature $T = 323$ K for 5 h. Glass substrates (1 cm × 1 cm) were cleaned by subsequent ultrasonic treatment in detergent, distilled water, acetone and isopropanol.

The glass substrates were spin-coated with the blend solution 800 rpm for 60 s, followed by 1000 rpm for 10 s after which they were dried at $T = 323$ K for at least 1 h on a hot plate. The resulting active layer thickness was ~230 nm, as determined by profilometry. Au electrodes capped with a layer of Al were deposited by thermal evaporation under high vacuum ($p \approx 1 \times 10^{-6}$ mbar) on top of the spin-coated films. A thin, wire-based shadow mask was used to create an inter-electrode gap of approximately 100 µm. All the above procedures, save for the cleaning of the substrates, were done in a glove box under $N_2$ atmosphere ($[O_2] <$ 1 ppm and $[H_2O] < 1$ ppm) or in an integrated thermal evaporator.

*Scanning Kelvin Probe Microscopy*: SKPM images were recorded in a glove box under $N_2$ atmosphere ($[O_2] < 1$ ppm and $[H_2O] < 1$ ppm) with a Veeco Instruments MultiMode AFM with Nanoscope IV controller, operating in lift mode with a lift height of 25 nm. Ti-Pt coated silicon tips (MikroMasch NSC36/Ti-Pt, $k$ ~1.75 N m$^{-1}$) were employed. All measurements were carried out at $T = 333$ K.

*UV-excited Photoluminescence Detection*: Optical probing was performed in an optical-access cryostat under high vacuum ($p <$ $10^{-5}$ mbar), using a single-lens reflex camera (Canon EOS50) equipped with a macro lens (focal length 65 mm) and a ×2 teleconverter. In parallel with the optical probing, the current was measured with a computer-controlled source-measure unit (Keithley 2612). Also the electro-optical probing was carried out at $T = 333$ K.

*Computational Details*: A 1-dimensional model was used in which an active layer of length $L = 20$ µm was divided in $N = 81$ discrete, equidistant points. The numerical model solves the drift-diffusion equations for electrons, holes, anions and cations, and Poisson's equation on this grid by forward integration in time. Devices with a bandgap $E_g = 2$ eV were simulated during operation at a bias voltage $V_{bias} = 5$ V until steady state had been reached, recognized by a zero ion current. A detailed description of the numerical model can be found in the Supplementary Information. Simulations were run for devices with initial ion concentrations $c_0$ varying between $1 \times 10^{-6}$ nm$^{-3}$ and $1 \times 10^{-1}$ nm$^{-3}$. No binding energy was assumed between anions and cations. The electrodes were ionically-blocking and electrons and holes were injected from the contacts according to a self-designed injection model that gives rise to field dependent injection. The model is described in detail in the Supporting Information and has the advantage that injection is not affected by grid-point spacing. The hole and electron injection barriers were set at 0.5 and 1.5 eV, respectively, to simulate an asymmetric device. Such an asymmetry is realistic for the actual LECs, which use Au for both the anode and cathode. Bimolecular electron-hole recombination was described by a Langevin process and the electrostatic potential was determined by Poisson's equation. Furthermore, energetic and spatial disorder, as present in real polymers, were omitted for convenience, as were charge traps. In addition, we set the relative dielectric constant $\varepsilon = 3$, the temperature $T = 300$ K, and the hole and electron mobility $\mu_{p/n} = 5 \times 10^{-11}$ m$^2$ V$^{-1}$ s$^{-1}$. Finally the anion and cation mobility were chosen to be $5 \times 10^{-12}$ m$^2$ V$^{-1}$ s$^{-1}$. The ion mobility does not affect the outcome at steady state; only the transient behavior of the calculated LECs is somewhat influenced by this parameter. For ion mobilities equal to or smaller than $\mu_{p/n}$, this influence is mainly quantitative, not qualitative. It was checked that the inter-electrode gap did not affect the outcome of the calculations in any non-trivial manner (See Supporting Information).

## Supporting Information

Supporting Information is available from the Wiley Online Library or from the author.

## Acknowledgements

M.K. and S.R. acknowledge financial support by the High Tech Systems and Materials (HTS&M) program of the Dutch ministry of economic affairs. L.E. and P.M. acknowledge the Swedish Research Council (VR) and Wenner-Gren stiftelserna for scientific financial support. L.E. is a `Royal Swedish Academy of Sciences Research Fellow' supported by a grant from the Knut and Alice Wallenberg Foundation.

Received: November 9, 2010
Revised: January 5, 2011
Published online: March 22, 2011

[1] Q. B. Pei, G. Yu, C. Zhang, Y. Yang, A. J. Heeger, *Science* **1995**, *269*, 1086.
[2] J. M. Leger, *Adv. Mater.* **2008**, *20*, 1212.
[3] L. Hu, G. Xu, *Chem. Soc. Rev.* **2010**, *39*, 3275.
[4] Q. B. Pei, Y. Yang, G. Yu, C. Zhang, A. J. Heeger, *J. Am. Chem. Soc.* **1996**, *118*, 3922.
[5] H. Shimotani, G. Diguet, Y. Iwasa, *Appl. Phys. Lett.* **2005**, *86*, 022104.
[6] Q. J. Sun, Y. F. Li, Q. B. Pei, *J. Disp. Technol.* **2007**, *3*, 211.
[7] O. Inganas, *Chem. Soc. Rev.* **2010**, *39*, 2633.
[8] J. Gao, J. Dane, *Appl. Phys. Lett.* **2003**, *83*, 3027.
[9] J. Gao, J. Dane, *Appl. Phys. Lett.* **2004**, *84*, 2778.
[10] P. Matyba, K. Maturova, M. Kemerink, N. D. Robinson, L. Edman, *Nat. Mater.* **2009**, *8*, 672.
[11] S. van Reenen, P. Matyba, A. Dzwilewski, R. A. J. Janssen, L. Edman, M. Kemerink, *J. Am. Chem. Soc.* **2010**, *132*, 13776.
[12] D. B. Rodovsky, O. G. Reid, L. S. C. Pingree, D. S. Ginger, *Acs Nano* **2010**, *4*, 2673.
[13] J. D. Slinker, J. A. DeFranco, M. J. Jaquith, W. R. Silveira, Y. W. Zhong, J. M. Moran-Mirabal, H. G. Craighead, H. D. Abruna, J. A. Marohn, G. G. Malliaras, *Nat. Mater.* **2007**, *6*, 894.

[14] C. Y. Lin, A. Garcia, P. Zalar, J. Z. Brzezinski, T. Q. Nguyen, *J. Phys. Chem. C* **2010**, *114*, 15786.
[15] Z. Chen, X. D. Dang, A. Gutacker, A. Garcia, H. P. Li, Y. H. Xu, L. Ying, T. Q. Nguyen, G. C. Bazan, *J. Am. Chem. Soc.* **2010**, *132*, 12160.
[16] G. Latini, G. Winroth, S. Brovelli, S. O. McDonnell, H. L. Anderson, J. M. Mativetsky, P. Samori, F. Cacialli, *J. Appl. Phys.* **2010**, *107*, 124509.
[17] L. He, L. A. Duan, J. A. Qiao, G. F. Dong, L. D. Wang, Y. Qiu, *Chem. Mat.* **2010**, *22*, 3535.
[18] R. Marcilla, D. Mecerreyes, G. Winroth, S. Brovelli, M. D. R. Yebra, F. Cacialli, *Appl. Phys. Lett.* **2010**, *96*, 043308.
[19] R. D. Costa, E. Orti, H. J. Bolink, S. Graber, C. E. Housecroft, E. C. Constable, *J. Am. Chem. Soc.* **2010**, *132*, 5978.
[20] J. Fang, P. Matyba, N. D. Robinson, L. Edman, *J. Am. Chem. Soc.* **2008**, *130*, 4562.
[21] T. Wågberg, P. R. Hania, N. D. Robinson, J. H. Shin, P. Matyba, L. Edman, *Adv. Mater.* **2008**, *20*, 1744.
[22] J. M. Leger, D. B. Rodovsky, G. R. Bartholomew, *Adv. Mater.* **2006**, *18*, 3130.
[23] S. Tang, K. Irgum, L. Edman, *Organic Electronics* **2010**, *11*, 1079.
[24] Z. B. Yu, M. L. Sun, Q. B. Pei, *J. Phys. Chem. B* **2009**, *113*, 8481.
[25] C. V. Hoven, H. P. Wang, M. Elbing, L. Garner, D. Winkelhaus, G. C. Bazan, *Nat. Mater.* **2010**, *9*, 249.
[26] I. V. Kosilkin, M. S. Martens, M. P. Murphy, J. M. Leger, *Chem. Mat.* **2010**, *22*, 4838.
[27] F. D. Lin, E. M. Walker, M. C. Lonergan, *J. Phys. Chem. Lett.* **2010**, *1*, 720.
[28] J. Gao, Y. F. Li, G. Yu, A. J. Heeger, *J. Appl. Phys.* **1999**, *86*, 4594.
[29] J. Gao, G. Yu, A. J. Heeger, *Appl. Phys. Lett.* **1997**, *71*, 1293.
[30] J. H. Shin, S. Xiao, A. Fransson, L. Edman, *Appl. Phys. Lett.* **2005**, *87*, 043506.
[31] J. Dane, C. Tracy, J. Gao, *Appl. Phys. Lett.* **2005**, *86*, 153509.
[32] J. F. Fang, P. Matyba, L. Edman, *Adv. Fun. Mater.* **2009**, *19*, 2671.
[33] J. F. Fang, Y. L. Yang, L. Edman, *Appl. Phys. Lett.* **2008**, *93*, 063503.
[34] Y. Shao, G. C. Bazan, A. J. Heeger, *Adv. Mater.* **2008**, *20*, 1191.
[35] A. Sandstrom, P. Matyba, L. Edman, *Appl. Phys. Lett.* **2010**, *96*, 053303.
[36] S. Tang, L. Edman, *J. Phys. Chem. Let.* **2010**, *1*, 2727.
[37] N. D. Robinson, J. F. Fang, P. Matyba, L. Edman, *Phys. Rev. B* **2008**, *78*, 245202.
[38] D. M. deLeeuw, M. M. J. Simenon, A. R. Brown, R. E. F. Einerhand, *Synth. Met* **1997**, *87*, 53.
[39] *Solid State Electrochemistry* (Ed: P. G. Bruce), Cambridge University Press **1995**.
[40] M. Marzantowicz, J. R. Dygas, F. Krok, A. Tomaszewska, G. Z. Zukowska, Z. Florjanczyk, E. Zygadlo-Monikowska, *Electrochim. Acta* **2010**, *55*, 5446.